

# Natural evolutionary strategies applied to quantum-classical hybrid neural networks

Lucas Friedrich<sup>1,\*</sup> and Jonas Maziero<sup>1,†</sup>

<sup>1</sup>*Departamento de Física, Centro de Ciências Naturais e Exatas,  
Universidade Federal de Santa Maria, Avenida Roraima 1000, 97105-900, Santa Maria, RS, Brazil*

With the rapid development of quantum computers, several applications are being proposed for them. Quantum simulations, simulation of chemical reactions, solution of optimization problems and quantum neural networks are some examples. However, problems such as noise, limited number of qubits and circuit depth, and gradient vanishing must be resolved before we can use them to their full potential. In the field of quantum machine learning, several models have been proposed. In general, in order to train these different models, we use the gradient of a cost function with respect to the model parameters. In order to obtain this gradient, we must compute the derivative of this function with respect to the model parameters. For this we can use the method called *parameter-shift rule*. This method consists of evaluating the cost function twice for each parameter of the quantum network. A problem with this method is that the number of evaluations grows linearly with the number of parameters. In this work we study an alternative method, called Natural Evolutionary Strategies (NES), which are a family of black box optimization algorithms. An advantage of the NES method is that in using it one can control the number of times the cost function will be evaluated. We apply the NES method to the binary classification task, showing that this method is a viable alternative for training quantum neural networks.

Keywords: Quantum Neural Networks, Natural Evolutionary Strategies, Quantum Binary Classification, Hybrid Quantum-Classical Neural Networks

## I. INTRODUCTION

Many developments in science and technology in last years were obtained with the aid of artificial intelligence. Its applications extend to the most varied areas of knowledge, such as computer vision [1–3], natural language processing [4, 5], drug discovery [6], analysis of astronomical images [7], and chemistry simulations [8]. With the development of quantum computers, several studies are being conducted with the aim of taking artificial intelligence to the quantum domain [16–23]. It is hoped that, by utilizing phenomena such as entanglement and superposition, we will be able to create models more powerful than their classical counterparts.

Models such as Quantum Multilayer Perceptron [9], Quantum Convolutional Neural Networks [10], Quantum Kernel Method [11], and Quantum-Classical Hybrid Neural Networks (HQCNN) [12–15] are some candidate models. In the era of noisy intermediate-scale quantum devices (NISQ), hybrid models are the most used. This era is characterized by the limited number of qubits we have access to and the presence of noise. Hybrid models are built using sequential classical and quantum layers. With this, we are able to create models with fewer qubits. For training these models, we can use the gradient descent method or its variants. The gradient descent method consists of using the gradient of a cost function to update the parameters of the neural network. To obtain the gradient of the quantum layers, one can use the method called *parameter-shift rule* (PSR), which consists of evaluating the cost function for each parameter of the quantum layers. As in current NISQ era the number of qubits that we have access to is limited and the depth of the parameterizations is also limited by noise and decoherence, the use of the PSR method is the most indicated, because with it we are able to obtain the derivatives of the cost function analytically. However, as quantum computers develop and the number of qubits and the depth of the parameterizations increase, this method tends to become impractical, being therefore necessary to find alternative ways for the task of training quantum neural networks.

Natural Evolutionary Strategies (NES) [26] are a family of black box optimization algorithms. These algorithms have already been applied to a variety of classical problems. For example, NES has been shown to be an alternative to reinforcement learning [27]. However, its application in the quantum domain is still scarce, and only a few works [28–30] were done for this purpose. Such a strategy is promising, because the number of evaluations of the cost function does not scale with the number of parameters. Furthermore, as the cost function evaluations are independent, this method can be parallelized.

---

\*Electronic address: [lucas.friedrich@acad.ufsm.br](mailto:lucas.friedrich@acad.ufsm.br)

†Electronic address: [jonas.maziero@ufsm.br](mailto:jonas.maziero@ufsm.br)

This article is organized as follows. In Sec. II, we review the HQCNN models, where a parallel is made with the classical deep neural network models. After that, in Sec. II A, we briefly discuss how classical layers work. In Sec. II B, we describe how a quantum layer works, and in Sec. II B 1 we discuss different ways of mapping classical data into quantum states. In the sequence, in Sec. II B 2, we discuss how the parameterization of a quantum layer is done. Finally, in Sec. II B 3, we describe how measurements can be made on HQCNN. In Sec. III, we present a review of the NES method, showing how to estimate the gradient of a given function. In Sec. IV, we start by describing the two HQCNN models that we use in this study. In Sec. IV B, we show how an HQCNN model is trained, and we present our training proposal using NES. In Sec. V, we briefly describe how the experiments are done, and, in Sec. VI, we present the results we obtained. Finally, in Sec. VII, we give our conclusions.

## II. QUANTUM-CLASSICAL HYBRID NEURAL NETWORKS

In recent years, classical deep neural network models, which is one of the branches of machine learning, have been responsible for a real revolution in the world. These models were applied to solve problems in the most varied areas of knowledge, such as classification, image and video analysis, fraud detection, recommendation systems and medical diagnosis. Furthermore, research on the application of deep learning to problems involving quantum mechanics and quantum computing has also been developed. These models are characterized by the use of several concatenated classical layers, that is, for a model with depth  $d$ , we have

$$C = L_{n_{d-1} \rightarrow n_d} \circ L_{n_{d-2} \rightarrow n_{d-1}} \circ \cdots \circ L_{n_1 \rightarrow n_2} \circ L_{n_0 \rightarrow n_1}, \quad (1)$$

where each  $L$  represents a classical layer and the first and second indices represent, respectively, the input size and the output size. HQCNN models are also characterized by the use of several concatenated layers, that is

$$\mathcal{Q} = \mathcal{L}_{n_{d-1} \rightarrow n_d} \circ \mathcal{L}_{n_{d-2} \rightarrow n_{d-1}} \circ \cdots \circ \mathcal{L}_{n_1 \rightarrow n_2} \circ \mathcal{L}_{n_0 \rightarrow n_1}, \quad (2)$$

where each  $\mathcal{L}$  represents a classical or quantum layer. We can see that the difference between classical deep neural network models and hybrid quantum-classical models is due to the addition of quantum layers to the classical model. It is expected that by using quantum layers together with classical layers we will be able to build models with greater power and accuracy than models using only classical layers.

### A. Classical Layer

The structures known as *layers* are one of the main building blocks of all modern classical deep neural network models. Such structures map an input of dimension  $n_0$  to an output of dimension  $n_1$ . A typical example of these structures is a linear transformation followed by a nonlinear activation function, defined by

$$\mathcal{L}_{n_0 \rightarrow n_1} = \phi(\mathbf{W}\mathbf{x} + \mathbf{b}), \quad (3)$$

where  $\mathbf{x}$  is an input vector with dimension  $n_0$ ,  $\mathbf{W}$  is an array with dimensions  $n_1 \times n_0$  and  $\mathbf{b}$  is a vector with dimension  $n_1$ . The elements of  $\mathbf{W}$  are real values that are updated throughout training. One of the key pieces of deep neural network models is the nonlinearity implemented by the  $\phi$  function. There are several functions that we can use to apply nonlinearity, such as the hyperbolic tangent, the Sigmoid or the Relu.

Furthermore, we can mention the neural network architecture with convolutional layers, which are mainly applied to problems involving computer vision, and the *Long short-term memory* (LSTM), which are used when dealing with problems related to time series, among many others.

### B. Quantum Layer

#### 1. Encoder

The first task when building a quantum layer is to encode the data of interest in quantum states. For this, we can use different strategies, such as the wave function encoder

$$|\mathbf{x}\rangle := \frac{1}{\|\mathbf{x}\|_2} \sum_{i=1}^{2^N} x_i |i\rangle, \quad (4)$$

the dense angle coding

$$|\mathbf{x}\rangle = \bigotimes_{i=1}^{N/2} \cos(\pi x_{2i-1})|0\rangle + e^{2\pi i x_{2i}} \sin(\pi x_{2i-1})|1\rangle, \quad (5)$$

or the qubit encoding

$$|\mathbf{x}\rangle = \bigotimes_{i=1}^N \cos(x_i)|0\rangle + \sin(x_i)|1\rangle. \quad (6)$$

The performance of quantum layers is influenced by this choice [31, 32, 35]. For example, in Ref. [32], it was shown that if we reload the data between the different layers of the parameterization, we will be able to create a model with greater classification capability.

## 2. Parameterization

After mapping the data of interest to a quantum state, the next step is to apply a parameterization that is generally given by

$$U(\boldsymbol{\theta}) = \prod_{i=1}^L U_i W_i, \quad (7)$$

with

$$U_i = \bigotimes_{j=1}^N R_{\sigma}^{j,i}(\theta_{j,i}), \quad (8)$$

where  $R_{\sigma}^{i,j}(\theta_{j,i}) = e^{-i\theta_{j,i}\sigma/2}$  with  $\sigma \in (\sigma_x, \sigma_y, \sigma_z)$  is one of the Pauli matrices and  $W_i$  are unparameterized gates.

There are several ways to build the parameterization, and different parameterizations have different expressiveness. Expressiveness is defined as the ability of a given parameterization to explore the Hilbert space. However, the relationship between this choice and the performance of the model is not direct. The parameterization most frequently used in the literature is the one defined in Eq. (7).

## 3. Measurements

After mapping the data of interest to a quantum state and applying the parameterization  $U(\boldsymbol{\theta})$ , Eq. (7), the next step is to perform the measurements. The measurements can be done globally, where all qubits are measured, or locally, where only a few qubits are measured individually or in pairs. As a result of these measurements, we can estimate the mean value

$$f_i = \text{Tr}[H_i \rho_x^{out}], \quad (9)$$

where  $H_i$  is a Hermitian operator and  $\rho_x^{out}$  is the density matrix at the end of the quantum circuit. That is, given an input  $|\mathbf{x}\rangle$  and a parameterization  $U(\boldsymbol{\theta})$ , Eq. (7), we have that  $\rho_x^{out} = U(\boldsymbol{\theta})|\mathbf{x}\rangle\langle\mathbf{x}|U(\boldsymbol{\theta})^\dagger$ .

A particular case is

$$H_i = |i\rangle\langle i|. \quad (10)$$

In this case, the outputs will be the respective probabilities of our circuit being in a state of the computational basis. This is a definition of what we can call a global measurement, where all qubits contribute to the value of  $f_i$ .

Another case is when we define  $H_i$  as

$$H_i = \mathbb{I}_{\bar{i}} \otimes |0\rangle\langle 0|. \quad (11)$$

Here the index  $\bar{i}$  indicates that the identity operator will be applied to all qubits with exception to the qubit with index  $i$ . The index  $i$  indicates that  $|0\rangle\langle 0|$  will be applied only to the qubit of index  $i$ . This is a definition for what we call local measurements, where only the qubit with index  $i$  contributes to the value of  $f_i$ . In this specific case, where  $|0\rangle\langle 0|$  is used, we will get the probability for the qubit  $i$  to be in the state  $|0\rangle$ .

### III. NATURAL EVOLUTIONARY STRATEGIES

Given a function  $f(\mathbf{z})$ , with  $\mathbf{z} \in \mathbb{R}^d$ , in the natural evolutionary strategy we reparameterize this function as follows:

$$J(\theta) = \mathbb{E}_\theta[f(\mathbf{z})] = \int f(\mathbf{z})\pi(\mathbf{z}|\theta)d\mathbf{z}. \quad (12)$$

By deriving Eq. (12) with respect to  $\theta$ , we get

$$\begin{aligned} \nabla_\theta J(\theta) &= \nabla_\theta \int f(\mathbf{z})\pi(\mathbf{z}|\theta)d\mathbf{z} \\ &= \int f(\mathbf{z})\nabla_\theta \pi(\mathbf{z}|\theta)d\mathbf{z} \\ &= \int f(\mathbf{z})\nabla_\theta \pi(\mathbf{z}|\theta) \frac{\pi(\mathbf{z}|\theta)}{\pi(\mathbf{z}|\theta)} d\mathbf{z} \\ &= \int [f(\mathbf{z})\nabla_\theta \log \pi(\mathbf{z}|\theta)]\pi(\mathbf{z}|\theta)d\mathbf{z} \\ &= \mathbb{E}_\theta[f(\mathbf{z})\nabla_\theta \log \pi(\mathbf{z}|\theta)]. \end{aligned} \quad (13)$$

Thus, we can estimate the gradient using

$$\nabla_\theta J(\theta) \approx \frac{1}{\lambda} \sum_{k=1}^{\lambda} f(\mathbf{z}_k) \nabla_\theta \log \pi(\mathbf{z}_k|\theta). \quad (14)$$

For the case of a Gaussian distribution

$$\pi(\mathbf{z}|\theta) = \frac{1}{(2\pi)^d \det \Sigma} \exp\left(-\frac{1}{2}(\mathbf{z} - \boldsymbol{\mu})^T \Sigma^{-1}(\mathbf{z} - \boldsymbol{\mu})\right), \quad (15)$$

with parameters  $\theta := \{\boldsymbol{\mu}, \Sigma\}$ . We have that  $\nabla_\theta \log \pi(\mathbf{z}|\theta)$  will be given by

$$\nabla_{\boldsymbol{\mu}} \log \pi(\mathbf{z}|\theta) = \Sigma^{-1}(\mathbf{z} - \boldsymbol{\mu}) \quad (16)$$

and

$$\nabla_{\Sigma} \log \pi(\mathbf{z}|\theta) = \frac{1}{2}\Sigma^{-1}(\mathbf{z} - \boldsymbol{\mu})(\mathbf{z} - \boldsymbol{\mu})^T \Sigma^{-1} - \frac{1}{2}\Sigma^{-1}. \quad (17)$$

The main NES methods use both Eq. (16) and Eq. (17) to obtain an estimate of Eq. (14). However, as in this study we will consider the Gaussian distribution given by  $\mathcal{N}(\boldsymbol{\theta}, \sigma^2 \mathbf{I})$ , i.e.,  $\boldsymbol{\mu} = \boldsymbol{\theta}$  and  $\Sigma = \sigma^2 \mathbf{I}$ , we will use only the Eq. (16), once  $\Sigma = \text{const.}$  Thus, from Eqs. (14) and (16), we get

$$\nabla_\theta J(\theta) \approx \frac{1}{\lambda \sigma^2} \sum_{k=1}^{\lambda} (\mathbf{z}_k - \theta) \cdot f(\mathbf{z}_k), \quad (18)$$

with  $\mathbf{z}_k \sim \mathcal{N}(\theta, \sigma^2 \mathbf{I})$ . The algorithm that implements Eq. (18).

**Input:**  $f(z)$ ,  $\theta$ ,  $\sigma$

**Output:**  $\nabla_\theta J(\theta)$

**for**  $k = 1 \dots \lambda$  **do**

$z_k \sim \mathcal{N}(\theta, \sigma^2 \mathbf{I})$   $f(z_k)$  ;

$\nabla_\theta J(\theta) = (z_k - \theta)$  ;

**end**

$\nabla_\theta J(\theta) \leftarrow \frac{1}{\lambda \sigma^2} \sum_{k=1}^{\lambda} (z_k - \theta) \cdot f(z_k)$  ;

*/\* Evaluates function  $f$  in  $z_k$  \*/*  
*/\* Calculates the derivative \*/*

*/\* Estimates the gradient \*/*

**Algorithm 1:** Gradient estimation using Eq. (18).

## IV. METHOD

### A. Models

For this study, we will use two HQCNN models. The first model will be built using two quantum layers. The second model will be built using two classical layers and a quantum layer. In this work, we define the cost function as

$$L(\Delta) := \frac{1}{N} \sum_j^N (y_i^j - \bar{y}_i^j)^2, \quad (19)$$

where  $y_i$  is the vector obtained at the end of the network given the input  $x_i$  and  $\bar{y}_i$  is the respective desired output. Here  $\Delta := \{\mathbf{W}, \boldsymbol{\theta}\}$  is defined as the set of network parameters.

#### 1. Model 1

The first layer will be built using five qubits, as illustrated in Fig. 1. Data will be mapped using real amplitudes as illustrated in Fig. 2. This is a parameterization used for machine learning and quantum chemistry problems. The parameterization will be given by  $U(\boldsymbol{\theta})$ , Eq. (7). In Fig. 3 shows how the parameterization is done for each  $U_i$ . For measurements we will use Eq. (9) with the Hermitian operator defined in Eq. (11) for the last three qubits.

For the second layer, three qubits are used. The function that will map our data into a quantum state is represented in Fig. 4. The parameterization used will also be given by  $U(\boldsymbol{\theta})$ , Eq. 7. For the measurements we use Eq. (9) with  $H_i$  defined in Eq. (11). In this case the last two qubits will be used.

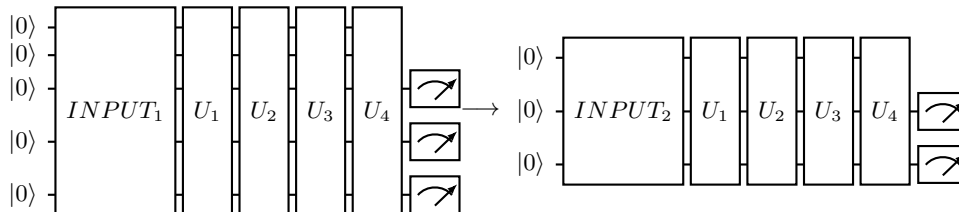


Figure 1: Model 1: Quantum-Classical Hybrid Neural Network.

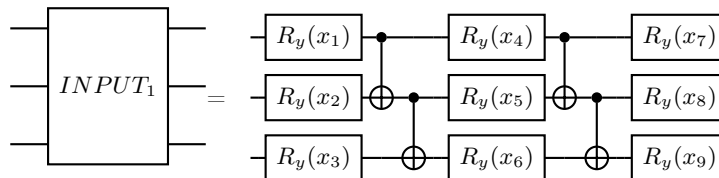


Figure 2:  $INPUT_1$  for the case of three qubits.

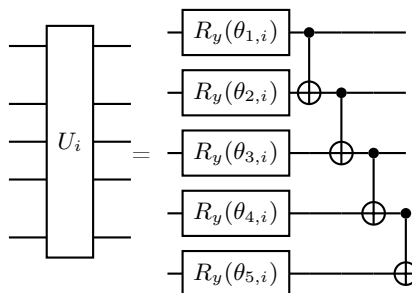


Figure 3: Parameterization of unitary operators  $U_i$ . See Figure 1.

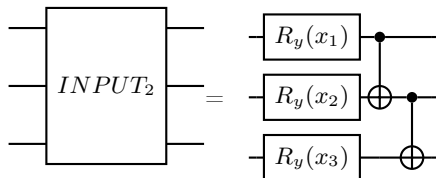


Figure 4:  $INPUT_2$  for the case of three qubits.

## 2. Model 2

The second model will be built using three layers. The first being a classical layer, the second is a quantum layer and the third is a second classical layer. In Eq. (3) we defined the classic layer that we will use. This consists of an operation that takes an input  $\mathbf{x}$  of size  $n$  into an output  $\mathbf{y}$  of size  $m$ , as illustrated in Fig. 5. In this study, as we will work with data from the *dataset* MNIST, which consists of images of dimension  $28 \times 28$ , the input of the first layer have size  $n = 784$ . The output data is encoded in the quantum layer using the parameterization model presented in Fig. 4, that is, for each qubit a value is encoded. Then the output of the first layer is equal in size to the number of qubits used in the quantum layer. For nonlinearity, the hyperbolic tangent function will be used.

The second layer, which is a quantum layer, is represented in Fig. 6. In this layer we use four qubits. Its parameterization will be given by  $U(\boldsymbol{\theta})$ , Eq. (7), with each  $U_i$  represented in Fig. 3. For measurements, we use Eq. (9) with the Hermitian operator defined in Eq. (11), with all qubits measured individually. The output of this quantum layer is used as input to a third layer, which is a classical layer, just like the first layer, with the difference being its size. The input of this third layer have dimension equal to the number of qubits used in the quantum layer and output  $m = 2$ .

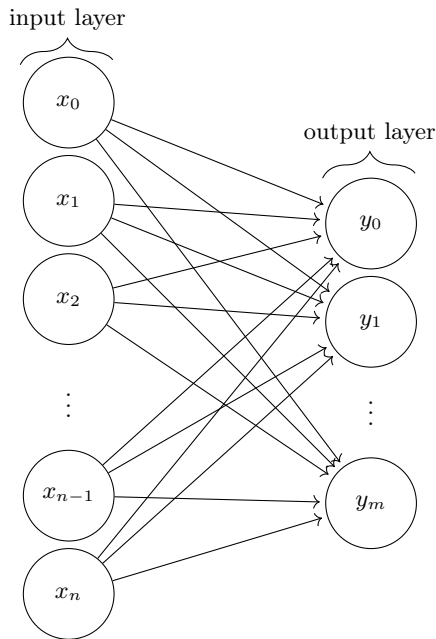


Figure 5: Linear Layer.

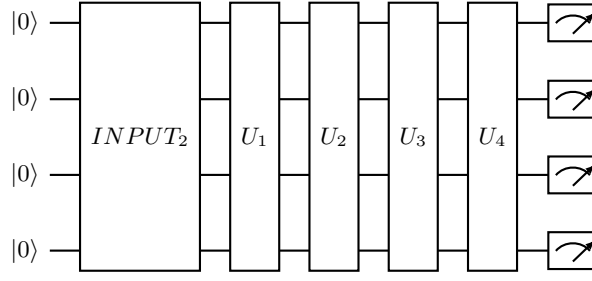


Figure 6: Quantum Layer.

## B. Training

Given  $\mathcal{D} := \{x_i, \bar{y}_i\}_{i=1}^n$ , a dataset, and defined the HQCNN model that shall be used, the training consists of an iterative method where, given an input  $x_i$  to the model, it returns an output  $y_i$ . Comparing this output to the desired output  $\bar{y}_i$ , we can compute the performance of our model using the cost function of Eq. (19). This process is performed iteratively for all data in the set  $\mathcal{D}$ , several times, or, as it is commonly called, for several epochs. During this process, we aim to minimize the cost function, that is,

$$\Delta_{opt} = \operatorname{argmin}_{\Delta} L(\Delta), \quad (20)$$

where  $\Delta_{opt}$  is the set of optimal parameters. To obtain  $\Delta_{opt}$ , at each iteration the  $\Delta$  parameters are updated generally using the gradient descent method or its variants. This method updates the parameters using the gradient of the cost function of Eq. (19). For this, we must use the chain rule. For example, let us consider the first model. Given an input  $x_i = (x_i^1, x_i^2, \dots, x_i^n)$  and its respective desired output  $\bar{y}_i = (\bar{y}_i^1, \bar{y}_i^2, \dots, \bar{y}_i^N)$ , the cost function is given by

$$L(\theta_1, \theta_2) = \frac{1}{N} \sum_{j=1}^N (\mathcal{L}_2(\mathcal{L}_1(x_i, \theta_1), \theta_2)^j - \bar{y}_i^j)^2, \quad (21)$$

where  $\mathcal{L}_1$  is the first layer with input  $x_i$  and parameters  $\theta_1$  and  $\mathcal{L}_2$  is the second layer with input given by the output of the first layer and with parameters  $\theta_2$ . Thus, the gradient of Eq. (19) in relation to the parameters  $\theta_1$  and  $\theta_2$  will be

$$\nabla_{\theta_2} L(\theta_1, \theta_2) = \frac{2}{N} \sum_j^N (\mathcal{L}_2(\mathcal{L}_1(x_i, \theta_1), \theta_2)^j - \bar{y}_i^j) \nabla_{\theta_2} \mathcal{L}_2(\mathcal{L}_1(x_i, \theta_1), \theta_2)^j, \quad (22)$$

$$\nabla_{\theta_1} L(\theta_1, \theta_2) = \frac{2}{N} \sum_j^N (\mathcal{L}_2(\mathcal{L}_1(x_i, \theta_1), \theta_2)^j - \bar{y}_i^j) \nabla_{\mathcal{L}_1} \mathcal{L}_2(\mathcal{L}_1(x_i, \theta_1), \theta_2)^j \nabla_{\theta_1} \mathcal{L}_1(x_i, \theta_1), \quad (23)$$

where in Eq. (23) the term  $\nabla_{\mathcal{L}_1}$  indicates that we must obtain the derivatives with respect to the input of the second layer. Using gradient descent as an example, from Eqs. (22) and (23) we have that the new parameters will be

$$\theta_1^{t+1} = \theta_1^t - \eta \nabla_{\theta_1} L(\theta_1, \theta_2) \quad (24)$$

and

$$\theta_2^{t+1} = \theta_2^t - \eta \nabla_{\theta_2} L(\theta_1, \theta_2) \quad (25)$$

where  $t$  represents the epoch and  $\eta$  the learning rate.

Consider the term  $\nabla_{\theta_1} \mathcal{L}_1(x_i, \theta_1)$  in Eq. (23). If we consider that this is a black box function, we can define  $J(\theta_1) := \mathcal{L}_1(x_i, \theta_1)$ . Here we can see that, up to an index, we can rewrite our quantum layer using Eq. (12). So, we can use Eq. (18) to estimate the gradient.

In Eq. (23), we see that we must also obtain the gradient with respect to the input data of the second layer. Again, we can consider the quantum layer to be a black box function with parameters given by  $(\mathcal{L}_1(x_i, \theta_1), \theta_2)$ . Therefore, we can again use Eq. (12) to describe this layer. Then the gradient can be estimated using Eq. (18).

### C. Barren Plateaus

The optimization of quantum circuits is done, in general, using the gradient in relation to its parameters. A current problem is the phenomenon known as gradient vanishing, or barren plateaus. Given a function

$$C = Tr[OU(\boldsymbol{\theta})|\mathbf{x}\rangle\langle\mathbf{x}|U(\boldsymbol{\theta})^\dagger], \quad (26)$$

if  $U(\boldsymbol{\theta})$  is a 2-*design*, then we have that

$$\langle\partial_k C\rangle = 0 \text{ and } Var[\langle\partial_k C\rangle] \approx 2^{-n}, \quad (27)$$

where  $n$  is the number of qubits. From the Chebyshev inequality,

$$Pr(|\partial_k C| \geq \delta) \leq \frac{Var[\langle\partial_k C\rangle]}{\delta^2}, \quad (28)$$

we have that the probability that  $\partial_k C$  deviates from its mean,  $\langle\partial_k C\rangle = 0$ , by a value  $\delta$  will tend to zero as the number of qubits increase.

Furthermore, results from the literature show that other factors also influence this phenomenon such as the choice of cost function [36], expressiveness of parameterization [37], noise [38] and entanglement [39, 40]. It is also shown that gradient vanishing is present in gradient free optimization methods [41]. In Fig. 7, we showed experimentally that this phenomenon is also observed when using the NES method. To obtain these results, we use the cost function

$$C = \frac{1}{n} \sum_{i=1}^n Tr[H_i U(\boldsymbol{\theta}) \rho U(\boldsymbol{\theta})^\dagger], \quad (29)$$

with  $U(\boldsymbol{\theta})$  defined in Eq. (7) and  $H_i$  is defined in Eq. (11). To encode the input data, we will use the parameterization shown in Fig. 4.

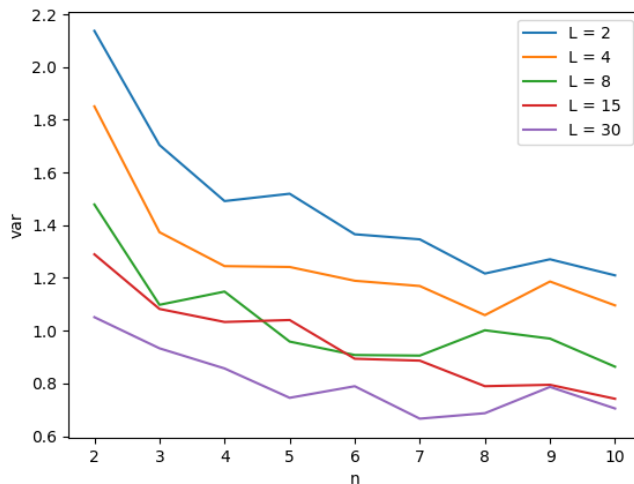


Figure 7: In this figure,  $n$  is the number of qubits used. For the input data,  $\mathbf{x} = (\pi/4, \pi/4, \pi/4, \dots, \pi/4)$  was used. We can see that as the number of qubits increases, the variance tends to decrease. Furthermore, we can also see that the variance decreases as the number of layers of the parameterization increases. Thus, we see that the phenomenon of gradient disappearance is also present in the NES method.

### V. EXPERIMENTS/SIMULATIONS

For this work, we will use Qiskit [42] and Pytorch [43] to build our models, with the Qiskit package integrated into Pytorch. With this, some steps such as the application of the chain rule to obtain the derivatives in Eqs. (22) and (23) and parameter optimization are done automatically by Pytorch. For training, 2000 training images are used,



half referring to zero digit images and half to the one digit images. For validation, 200 images are used, again half of each type. We also vary the value of the learning rate to see how the cost function behaves. Also, we perform the same experiment  $N$  times for obtaining the statistics. So, we can see how the NES method behaves for different initializations. Also, for this study we used  $\sigma = \frac{\pi}{24}$  for all cases. For the first experiments, we used

$$\lambda = 4 + 3 \log(p), \quad (30)$$

where  $p$  is the number of parameters of the respective quantum layer. For the layers where we should get the gradient for the input data, we use the highest value of  $\lambda$ . That is, given the value of  $\lambda$  for the layer's input data and parameters, we will use the largest of them.

As this is a method where we can control the number of times the function is evaluated, we will study how HQCNN models behave for different values of  $\lambda$ . Again, we run the same experiment  $N$  times so we can see how the NES method behaves for different initializations.

## VI. RESULTS

For the first experiment, two quantum circuits were used, Model 1 in Fig. 1. For this experiment and the following ones, the MNIST data set was used, and only part of the data was used. Once the model that will be used is created, it was defined that for the optimization we will use the Adam optimizer with a learning rate,  $\eta$ , variable. We start using  $\eta = 0.01$ . Up to 100 epochs were used for training. For each value of the learning rate, the same experiment was repeated four times. For each new training, the parameters were randomly initialized. With this we can see how the NES method behaves for each initialization.

In Fig. 8, we can see that if we use  $\eta = 0.01$ , the neural network will reach a point where it will be stuck in a local minimum, that is, it will no longer be able to learn. For  $\eta = 0.001$ , we see that the neural network can learn as the epochs go by. In the case where  $\eta = 0.0001$  was used, we see that for this number of epochs used, the neural network performed worse than in the other cases. But we can see that even as the epochs passed, the network was able to learn without getting stuck in a local minimum, as was the case for  $\eta = 0.01$ .

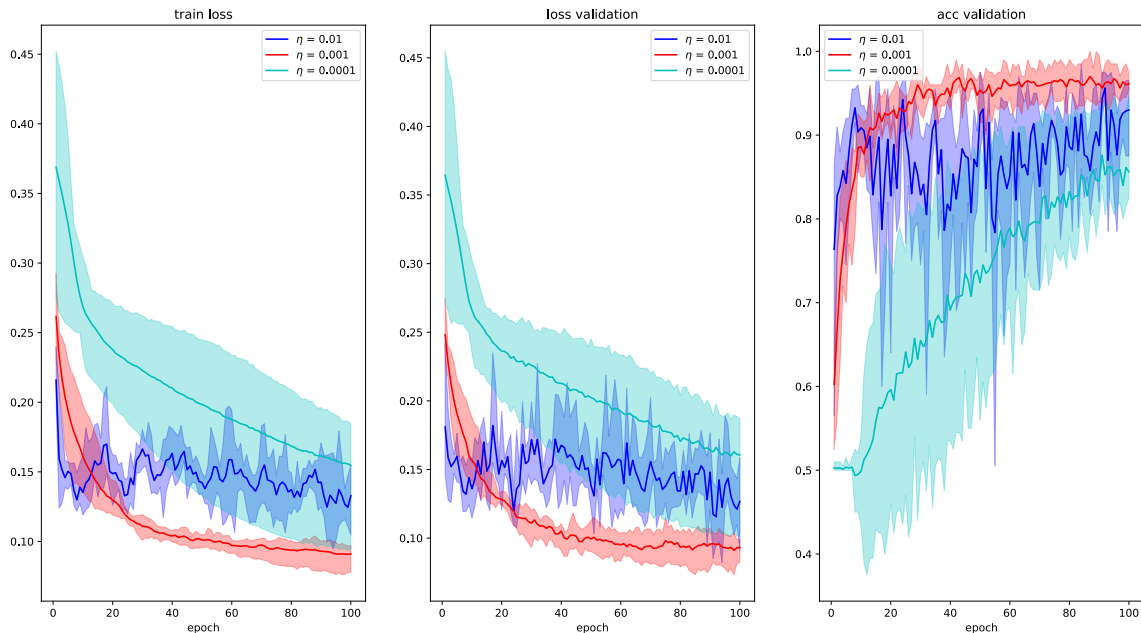


Figure 8: Result for model 1. In darker colors the means for  $N = 4$  experiments are shown. The lighter colors represent values between the minimum and maximum values. To obtain the gradient estimate, the Algorithm 1 was used. In order to be able to update the parameters of the first layer, we must get the gradient from the input data of the second layer. For this we can also use the Algorithm 1, with  $\theta$  being the input data in this case.

For the results presented in Fig. 9, the only difference from the previous one was the model used, in this case the Model 2. The training and validation datasets are the same as in the previous case. Again we use the Adam optimization with variable learning rate. Unlike the previous model, we see that for both  $\eta = 0.01$  and  $\eta = 0.001$ ,

the neural network was stuck in a local minimum, being unable to learn. The neural network was only able to learn when we used  $\eta = 0.0001$ , where we can see that it quickly converged to the desired minimum.

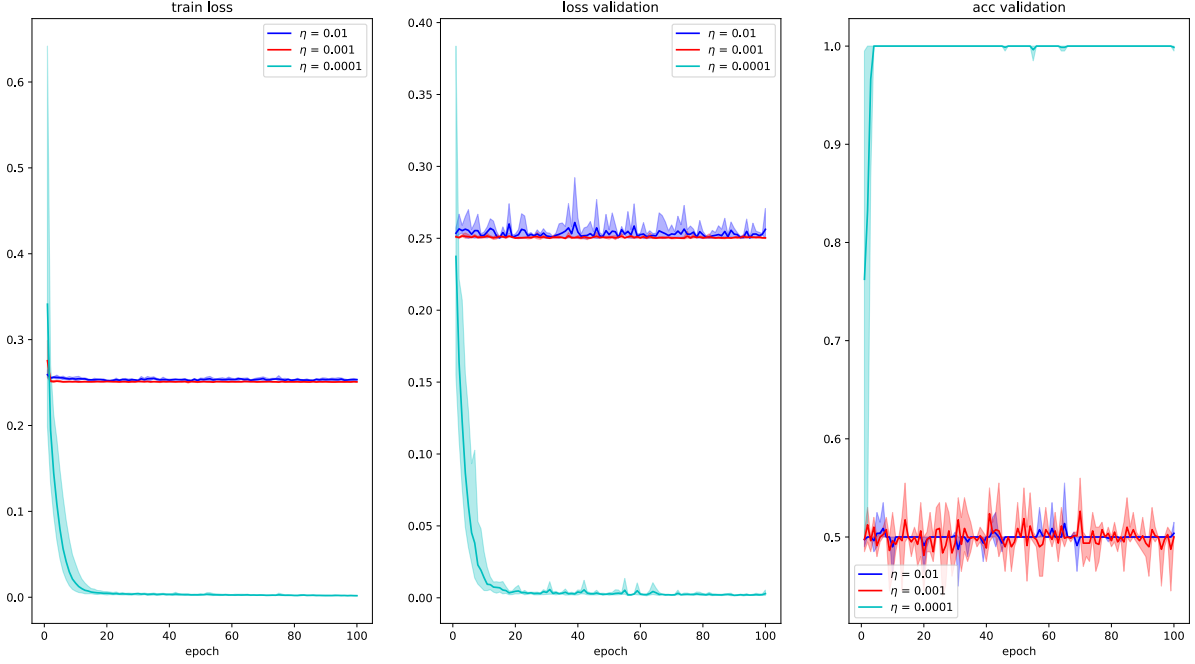


Figure 9: Results for Model 2. The means for  $N = 4$  experiments are shown in darker colors, while the lighter colors represent values between the minimum and maximum values. Algorithm 1 was used to obtain the gradient estimate. To update the parameters of the first layer, we must get the gradient from the input data of the second layer. For this we can also use the Algorithm 1, with  $\theta$  being the input data in this case.

In the next graphs, in Figs. 10 and 11, Models 1 and 2 were used, respectively, with the data set defined as in the previous experiments, and with a variable learning rate. In these two cases, the difference lies in the number of times the cost function is evaluated, that is to say, the value of  $\lambda$  that is used to estimate the gradient, Eq. (18). In the first case, using two quantum layers, Fig. 10, we see that using  $\eta = 0.01$  the neural network was not able to learn for any value of  $\lambda$ . For  $\eta = 0.001$ , its behavior was similar for all values of  $\lambda$ . As for  $\eta = 0.0001$ , its behavior was not better than using  $\eta = 0.001$ , but we can see that the neural network was able to learn over the epochs for all values of  $\lambda$ .

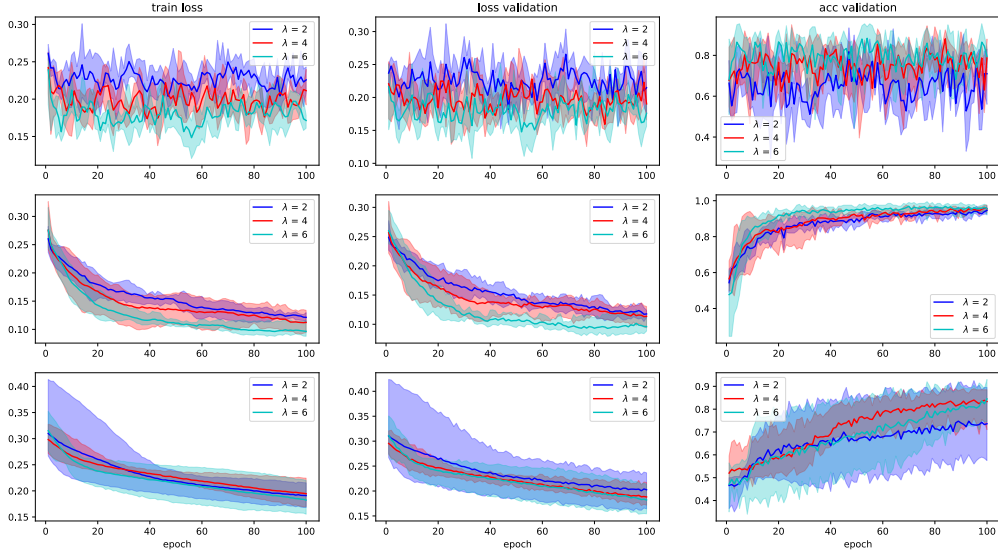


Figure 10: Results for Model 1 with variable  $\lambda$  and learning rate  $\eta$ . In darker colors, the averages for  $N = 4$  experiments are shown. The lighter colors represent values between the minimum and maximum values. In the upper figures,  $\eta = 0.01$  was used. In the 2nd row figures we used  $\eta = 0.001$ , and in the lower figures we used  $\eta = 0.0001$ .

In this second case, from Fig. 11, where we use Model 2, we see that its behavior was only satisfactory for  $\eta = 0.0001$ , and in other cases the neural network was not able to learn. With this, we can see experimentally that the performance of the NES method applied in hybrid quantum-classical models, where both classical and quantum layers are used, Model 2 has greater dependence on its hyperparameters.

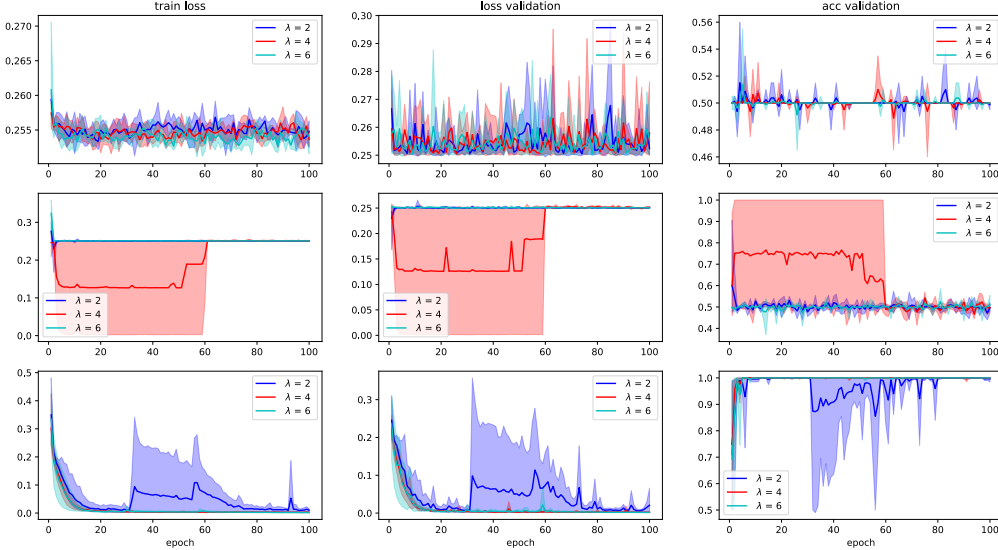


Figure 11: Results for Model 2 with variable  $\lambda$  and learning rate  $\eta$ . In darker colors the averages for  $N = 4$  experiments are shown. The lighter colors represent values between the minimum and maximum values. In the upper figures,  $\eta = 0.01$  was used. In the 2nd row figures, we used  $\eta = 0.001$ , and in the lower figures we used  $\eta = 0.0001$ .

### VII. CONCLUSIONS

In this work, we aimed to show the application of the Natural Evolutionary Strategies (NES) method in the training of Hybrid Quantum-Classical Neural Networks (HQCNN) models. For this, two different models were used. The first model was built using two quantum layers and the second model was built using classical and quantum layers together. For the application of the NES method, the chain rule was used in the cost function, where the NES method was used

to obtain an estimate of the gradient in relation to the quantum layers. From the results obtained, we saw that the choice of the learning rate has a significant influence on the behavior of the cost function. For example, for the first model, the best behavior was obtained with  $\eta = 0.001$ . For the second model we saw that for  $\eta = 0.01$  and  $\eta = 0.001$ , the HQCNN was not able to learn. However, for  $\eta = 0.0001$  it quickly converged to the desired minimum of the cost function. We also saw how the NES method behaves for different evaluation values of the cost function. Furthermore, as in the NISQ era the number of qubits we are able to simulate is limited, further work on the application of the NES method for optimizing HQCNN models with a higher number of qubits should be done.

### Acknowledgments

This work was supported by the Fundação de Amparo à Pesquisa do Estado do Rio Grande do Sul (FAPERGS) and by the Instituto Nacional de Ciência e Tecnologia de Informação Quântica (INCT-IQ), process 465469/2014-0.

**Data availability** The Qiskit/Pytorch code used for implementing the simulations to obtain the data used in this article is available upon request to the authors.

- 
- [1] K. He, X. Zhang, S. Ren, and J. Sun, Deep residual learning for image recognition, *Proceedings of the IEEE Conference on Computer Vision and Pattern Recognition* (2016).
  - [2] C. Szegedy et al., Going deeper with convolutions, *Proceedings of the IEEE Conference on Computer Vision and Pattern Recognition* (2015).
  - [3] A. Voulodimos, N. Doulamis, A. Doulamis, and E. Protopapadakis, Deep Learning for Computer Vision: A Brief Review, *Computational Intelligence and Neuroscience*, 2018, e7068349 (2018).
  - [4] J. Devlin, M.-W. Chang, K. Lee, and K. Toutanova, Bert: Pre-training of deep bidirectional transformers for language understanding, <https://doi.org/10.48550/arXiv.1810.04805> (2018).
  - [5] I. Sutskever, O. Vinyals, and Q. V. Le, Sequence to sequence learning with neural networks, *Advances in Neural Information Processing Systems* 27 (2014).
  - [6] J. Vamathevan et al., Applications of machine learning in drug discovery and development, *Nature Reviews Drug Discovery* 18, 463 (2019).
  - [7] Rodrigo Carrasco-Davis et al, Deep learning for image sequence classification of astronomical events, *Publications of the Astronomical Society of the Pacific*, 131, 108006 (2019).
  - [8] T.F.G.G. Cova and A.A.C.C. Pais, Deep learning for deep chemistry: optimizing the prediction of chemical patterns, *Frontiers in chemistry* 7, 809 (2019).
  - [9] C. Shao, A quantum model for multilayer perceptron, <https://doi.org/10.48550/arXiv.1808.10561> (2018).
  - [10] S.J. Wei, Y.H. Chen, Z.R. Zhou, and G.L. Long, A quantum convolutional neural network on NISQ devices, *AAPPS Bull.* 32, 2 (2022).
  - [11] M. Schuld, Supervised quantum machine learning models are kernel methods, <https://doi.org/10.48550/arXiv.2101.11020> (2021).
  - [12] J. Liu et al., Hybrid quantum-classical convolutional neural networks, *Sci. China Phys. Mech. Astron.* 64, 290311 (2021).
  - [13] Y. Liang, W. Peng, Z.-J. Zheng, O. Silvén, and G. Zhao, A hybrid quantum-classical neural network with deep residual learning, *Neural Networks* 143, 133 (2021).
  - [14] R. Xia and S. Kais, Hybrid quantum-classical neural network for calculating ground state energies of molecules, *Entropy* 22, 828 (2020).
  - [15] E. H. Houssein, Z. Abohashima, M. Elhoseny, and W. M. Mohamed, Hybrid quantum convolutional neural networks model for COVID-19 prediction using chest X-Ray images, *Journal of Computational Design and Engineering* 9, 343 (2022).
  - [16] S. Garg and G. Ramakrishnan, Advances in quantum deep learning: An overview, <https://doi.org/10.48550/arXiv.2005.04316> (2020).
  - [17] N. A. Nghiem, S. Y.-C. Chen, and T.-C. Wei, A Unified Framework for Quantum Supervised Learning, *Phys. Rev. Research* 3, 033056 (2021) 2020.
  - [18] E. Farhi and H. Neven, Classification with Quantum Neural Networks on Near Term Processors, <https://doi.org/10.48550/arXiv.1802.06002> (2018).
  - [19] F. Tacchino, P. Barkoutsos, C. Macchiavello, I. Tavernelli, D. Gerace, and D. Bajoni, Quantum implementation of an artificial feed-forward neural network, *Quantum Sci. Technol.* 5, 044010 (2020).
  - [20] G. Verdon, J. Pye, and M. Broughton, A Universal Training Algorithm for Quantum Deep Learning, <https://doi.org/10.48550/arXiv.1806.09729> (2018).
  - [21] K. Beer, D. Bondarenko, T. Farrelly, T. J. Osborne, R. Salzmann, D. Scheiermann, and R. Wolf, Training deep quantum neural networks, *Nature Comm.* 11, 808 (2020).
  - [22] S. Wei, Y. Chen, Z. Zhou, and G. Long, A Quantum Convolutional Neural Network on NISQ Devices, <https://doi.org/10.48550/arXiv.2104.06918> (2021).

- [23] S. Lloyd, M. Schuld, A. Ijaz, J. Izaac, and N. Killoran, Quantum embeddings for machine learning, <https://doi.org/10.48550/arXiv.2001.03622> (2020).
- [24] M. Cerezo, A. Arrasmith, R. Babbush, S. C. Benjamin, S. Endo, K. Fujii, J. R. McClean, K. Mitarai, X. Yuan, L. Cincio, and P. J. Coles, Variational quantum algorithms, *Nature Rev. Phys.* 3, 625 (2021).
- [25] M. Schuld, V. Bergholm, C. Gogolin, J. Izaac, and N. Killoran, Evaluating analytic gradients on quantum hardware, *Phys. Rev. A* 99, 032331 (2019).
- [26] D. Wierstra et al., Natural evolution strategies, *Journal of Machine Learning Research* 15, 949 (2014).
- [27] G. E. Crooks, Gradients of parameterized quantum gates using the parameter-shift rule and gate decomposition, <https://doi.org/10.48550/arXiv.1905.13311> (2019).
- [28] J. Yao, M. Bukov, and L. Lin, Policy Gradient based Quantum Approximate Optimization Algorithm, <https://doi.org/10.48550/arXiv.2002.01068>.
- [29] A. Anand, M. Degroote, and A. Aspuru-Guzik, Natural evolutionary strategies for variational quantum computation, *Mach. Learn.: Sci. Technol.* 2, 045012 (2021).
- [30] M. Wilson, S. Stromswold, F. Wudarski, S. Hadfield, N. M. Tubman, and E. Rieffel, Optimizing quantum heuristics with meta-learning, *Quantum Mach. Intell.* 3, 13 (2021).
- [31] M. Schuld, R. Sweke, and J. J. Meyer, The effect of data encoding on the expressive power of variational quantum machine learning models, *Phys. Rev. A* 103, 032430 (2021).
- [32] A. Pérez-Salinas, A. Cervera-Lierta, E. Gil-Fuster, and J. I. Latorre, Data re-uploading for a universal quantum classifier, *Quantum* 4, 226 (2020).
- [33] V. Bergholm et al., PennyLane: Automatic differentiation of hybrid quantum-classical computations, <https://doi.org/10.48550/arXiv.1811.04968> (2018).
- [34] M. Broughton et al., TensorFlow Quantum: A Software Framework for Quantum Machine Learning, <https://doi.org/10.48550/arXiv.2003.02989> (2020).
- [35] R. LaRose and B. Coyle, Robust data encodings for quantum classifiers, *Phys. Rev. A* 102, 032420 (2020).
- [36] M. Cerezo, A. Sone, T. Volkoff, L. Cincio, and P. J. Coles, Cost function dependent barren plateaus in shallow parametrized quantum circuits, *Nature Communications* 12, 1 (2021).
- [37] Z. Holmes, K. Sharma, M. Cerezo, and P. J. Coles, Connecting ansatz expressibility to gradient magnitudes and barren plateaus, *PRX Quantum* 3, 010313 (2022).
- [38] S. Wang et al., Noise-induced barren plateaus in variational quantum algorithms, *Nature Communications* 12, 6961 (2021).
- [39] C. O. Marrero, M. Kieferová, and N. Wiebe, Entanglement-induced barren plateaus, *PRX Quantum* 2, 040316 (2021).
- [40] T. L. Patti, K. Najafi, X. Gao, and S. F. Yelin, Entanglement devised barren plateau mitigation, *Phys. Rev. Research* 3, 033090 (2021).
- [41] A. Arrasmith, M. Cerezo, P. Czarnik, L. Cincio, and P. J. Coles, Effect of barren plateaus on gradient-free optimization, *Quantum* 5, 558 (2021).
- [42] D. C. McKay et al., Qiskit Backend Specifications for OpenQASM and OpenPulse Experiments, <https://doi.org/10.48550/arXiv.1809.03452> (2018).
- [43] A. Paszke et al., PyTorch: An Imperative Style, High-Performance Deep Learning Library, <https://doi.org/10.48550/arXiv.1912.01703> (2019).